Article

Quantifying acute fuel and respiration dependent pH homeostasis in live cells using the mCherryTYG mutant as a fluorescence lifetime sensor

Emily P. Haynes, Megha Rajendran, Chace K. Henning, Abhipri Mishra, Angeline M. Lyon, and Mathew Tantama

Anal. Chem., **Just Accepted Manuscript** • DOI: 10.1021/acs.analchem.9b01562 • Publication Date (Web): 05 Jun 2019

Quantifying acute fuel and respiration dependent pH homeostasis in live cells using the mCherryTYG mutant as a fluorescence lifetime sensor.

Emily P. Haynes[1], Megha Rajendran[1,2,†], Chace K. Henning[‡], Abhipri Mishra[‡], Angeline M. Lyon[1,3,4], Mathew Tantama[1,2,3]*

[1]Department of Chemistry, [2]Institute for Integrative Neuroscience, [3]Institute of Inflammation, Immunology, and Infectious Disease, [4]Department of Biological Sciences, Purdue University, 560 Oval Drive, Box 68, West Lafayette, IN 47907, USA.

ABSTRACT: Intracellular pH plays a key role in physiology, and its measurement in living specimens remains a crucial task in biology. Fluorescent protein-based pH sensors have gained widespread use, but there is limited spectral diversity for multicolor detection, and it remains a challenge to measure absolute pH values. Here we demonstrate that mCherryTYG is an excellent fluorescence lifetime pH sensor that significantly expands the modalities available for pH quantification in live cells. We first report the 1.09 Å X-ray crystal structure of mCherryTYG, exhibiting a fully matured chromophore. We next determine that it has an extraordinarily large dynamic range with a 2 nanosecond lifetime change from pH 5.5 to pH 9.0. Critically, we find that the sensor maintains a pKa of 6.8 independent of environment, whether as the purified protein in solution or expressed in live cells. Furthermore, the lifetime measurements are ro-bustly independent of total fluorescence intensity and scatter. We demonstrate that mCherryTYG is a highly effective sensor using time resolved fluorescence spectroscopy on live-cell suspensions, which has been previously overlooked as an easily accessible approach for quantifying intracellular pH. As a red fluorescent sensor, we also demonstrate mCherryTYG is spectrally compatible with the ATeam sensor and EGFP for simultaneous dual-color measurements of intracellular pH, ATP, and extracellular pH. In a proof-of-concept, we quantify acute respiration-dependent pH homeostasis that exhibits a stoichiometric relationship with the ATP-generating capacity of the carbon fuel choice in E. coli. Broadly speaking, our work presents previously unemployed methodology that will greatly facilitate continuous pH quantification.

The measurement of fluorescence lifetime is one of the most important approaches to obtaining quantitative information from endogenous or exogenous reporters in biological specimens[1,2]. However, fluorescence lifetime-based pH sensors have not been widely developed compared to fluorescence intensity or ratiometric probes. New approaches to live-specimen measurement are important because pH is a fundamental physiological parameter that is relevant to molecular biology[3], microbiology[4–7], cancer biology[8], neuroscience[9], and immunology[10] with applications in drug delivery[11] and bioproduction[7,12]. For example, in microbiology the proper measurement of pH remains key to answering open questions about homeostasis, environmental adaptation, and antibiotic resistance mechanisms in pathogenic bacteria such as *Escherichia coli*[4,13–16]. Measurements of cellular pH have provided insights into the underlying microbial physiology. For example, how decarboxylases, sigma factor, and other stress response systems enable *E. coli* to survive the acidic and basic environments of the mammalian gut[4,13–16]. These studies in turn provide foundations for the growing understanding that metabolic factors, such as respiratory capacity and proton motive force, contribute to the action of different types of antimicrobials[17,18]. In many of these studies, extracellular pH is monitored with electrodes or other physiochemical methods, with a growing use of fluorescent sensors to measure intracellular pH in living cells.

Fluorescent pH sensors have long been important in deciphering the physiology of prokaryotes and eukaryotes[19–21]. Small pH-sensitive organic dyes such as BCECF and SNARF[22] have been widely used, but dye loading, leakage, and non-specific binding to proteins and membranes can limit their application. In contrast, pH sensors based on fluorescent proteins (FPs) have grown in popularity because they are genetically-encoded and can be used in a range of cell types and species with targeting ability to organelles and subcellular locations. However, current FP-based pH sensors still need improvement. For example, commonly-used sensors, such as pHluorin and SypHer, utilize green and yellow FP variants[23,24]. Unfortunately, their color overlaps with the color of most other fluorescent sensors, precluding multiplexed experiments with more than one probe[21]. Therefore, it is important to develop new red fluorescent protein (RFP) pH sensors, but only a few have been developed thus far[25–29]. Furthermore, the current FP pH sensors rely on single-channel intensity or two-channel ratio readouts. Single-channel intensity sensors such are excellent for detecting events such as vesicle release in which large pH changes occur[30], but they are not ideal for quantifying pH due to high signal variability with expression level. Ratiometric sensors overcome this problem by normalizing for expression level via the ratio of two distinct spectral peaks. However, the ratio can depend on excitation power and filter bandwidths, and they occupy a

greater spectral space that can also limit multiplex measurements.

In contrast, fluorescence lifetime is an intrinsic property that offers a single-channel measurement that is independent of sensor concentration. Notably, lifetime measurements have proven highly robust and reproducible across different labs using different instrumentation, which facilitates direct quantitative comparisons of results between studies[31]. One challenge, however, is that the application of fluorescence lifetime sensing in biology turned its focus toward fluorescence lifetime imaging microscopy (FLIM) early on[32,33]. FLIM offers great spatial resolution and molecular specificity for a number of analytes[34,35] including protons[28,36–38], but in practice it is not yet a widely accessible technique because of the requirement for expensive commercial or custom-built systems. However, in many studies, high spatial resolution is not required to obtain critical understanding of live-cell physiology, and population measurements are entirely sufficient. Important alternative techniques are being developed, such as fluorescence lifetime flow cytometry and microfluidic methods[39,40]. Alternatively, steady-state spectroscopy of live-cell suspensions has proven highly effective for studying the physiology of in bacteria[41–43], yeast[44,45], and mammalian cells[46,47], but the time-resolved modality has not been exploited until now.

In this study, we demonstrate mCherryTYG can quantitatively report pH in live cells with its fluorescence lifetime. Although wildtype mCherry is pH insensitive, it is the most widely used RFP and has low cytotoxicity, thus providing an appropriate scaffold for an RFP pH sensor[48]. The M66T mutant, mCherryTYG, is pH sensitive[27] but it has not yet been used as a quantitative sensor. We find that it matures efficiently, corroborated by a high-resolution crystal structure that we obtained showing clear electron density for its chromophore. With solution and live cell studies, we demonstrate that this sensor exhibits an incredibly large dynamic range with a 2 ns lifetime change from pH 5 to 9. In a further demonstration of its applications, we use mCherryTYG to show that bacterial pH regulation is acutely dependent on fuel and aerobic respiration, using live cell suspension cultures with single-color and dual-color multiplexed measurements for the first time.

EXPERIMENTAL SECTION

Materials. Unless otherwise noted, chemicals were purchased from Sigma Aldrich, enzymes were purchased from New England Biolabs (NEB), and cell culture media and supplements were purchased from ThermoFischer (Invitrogen).

Protein Expression and Purification. Histidine-tagged wildtype mCherry gene was mutated to mCherryTYG using the NEB Q5 Mutagenesis kit, expressed in BL21(DE3) E. coli, and purified by nickel-affinity chromatography. Additional details are available in the Supporting Methods.

Crystallization. Crystals were obtained by hanging drop vapor diffusion experiments at 25 °C. Optimal crystallization conditions contained an equal volume of mCherryTYG at 10 mg/mL and well solution containing 50 mM Tris at pH 8.5, 100 mM sodium acetate, and 30% PEG 4000. Crystals were harvested on nylon loops and flash frozen in liquid N_2. X-ray diffraction data was collected at 100 K with an Eiger detector at the Advanced Photon Source LS-CAT 21-ID-D. HKL2000 was used for data integration and scaling. Phaser[49] was used to solve the structure by molecular replacement using the mCherry structure (PDB 2H5Q)[50] as a search model. Manual model building was performed in COOT[51] and altered with refinement in PHENIX[52]. The correctness of the final structure was determined using MolProbity[52]. Structure figures were generated using PyMol.

Steady-State Fluorescence Spectroscopy. pH titrations were performed by diluting protein to 0.2 - 1 μM in assay buffer containing 50 mM Tris, 50 mM Bis-Tris, 50 mM MOPS adjusted to pH 5.5 - 9.0 with NaOH or HCl.

Time-Resolved Spectroscopy with Purified Protein. The mCherryTYG protein samples were diluted to 0.2 - 1 μM in assay buffer. Fluorescence decays were measured by time-correlated single-photon counting (TCSPC) on a FS5-TCSPC+ (Edinburgh Instruments) with a Fianium WhiteLaseMicro supercontinuum laser (20 MHz repetition rate). All mCherryTYG lifetimes were measured with 546/10nm excitation and 580/10 nm emission. Typically, a neutral density filter was used to adjust count rates to 100,000 to 200,000 counts per second to avoid photon pileup artifacts, and typically at least 1,000,000 total photons were counted for peak counts of 1,000 - 5,000 photons to obtain well-defined decays. The instrument response function (IRF) was measured using LUDOX suspensions, and IRFs were collected to match total counting time and background counts of the fluorescent samples. Lifetime decay time constants were calculated by reconvolution fitting using the Fluoracle software (Edinburgh Instruments), and the lifetime value was calculated as the weighted average of the decay time constants. The pK_a values were determined by fitting pH data to a Boltzmann function.

Time-Resolved Spectroscopy with Live Cells Suspensions. Leaky expression of the fluorescent protein sensors was sufficient for live-cell experiments in DH5α *E. coli*. Bacteria were washed and diluted to an OD of 0.3 - 0.5 in 1.5 mL of continuously stirred M63 minimal medium (0.4 g/L KH_2PO_4, 2 g/L $(NH_4)_2SO_4$, 7.45 g/L KCl) buffered to the desired pH with 50 mM MES for pH 5.5 to 6.5, MOPS for pH 7.0 to 7.5, and Tris for pH 8.0 to 9.0. For live-cell pH calibration curves, IRFs were measured and reconvolution fitting was carried out to determine the lifetimes. For time course experiments, the empirical tail mean lifetime was measured to facilitate automated analysis. Empirical tail mean lifetimes were calculated as the photon count-weighted average lifetime for the 15 ns window after the peak. The pH calibration curve for the empirical mean lifetime (**Figure S4**) is comparable to the lifetimes obtained by IRF reconvolution fitting. Live-cell suspension treatments were added directly to stirring suspensions at final concentrations of 10 mM glucose, 10 mM KCN, 0.8% glycerol, and 40 mM benzoate and 40 mM methylamine. For simultaneous measurements of intracellular ATP and pH, cells expressing mCherryTYG and ATeam1.03YEMK were mixed. The ATeam1.03YEMK CFP donor lifetime was measured using 435/10 nm excitation with 485/10 nm emission. For simultaneous measurements of intracellular and extracellular pH, cells expressing mCherryTYG were diluted in M63 media containing 50 - 100

nM purified EGFP protein. The EGFP lifetime was measured using 475/10 nm excitation and 510/10 nm emission.

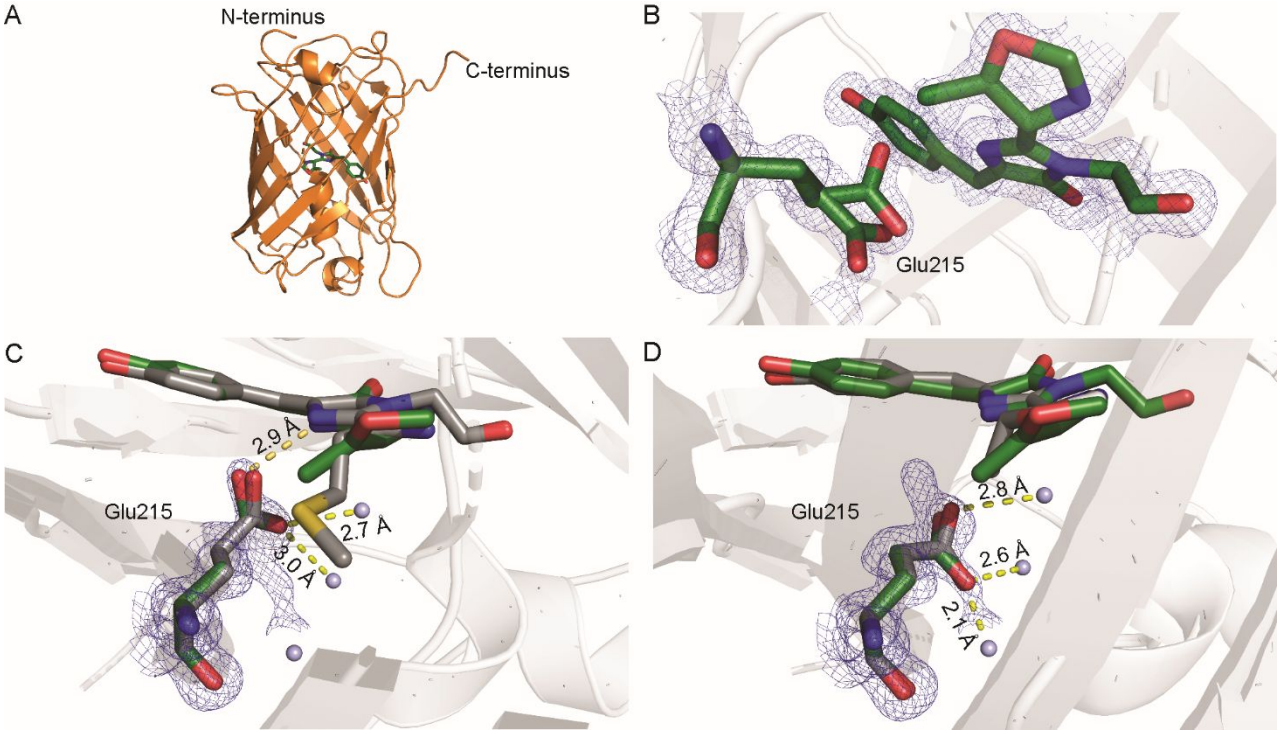

Figure 1. The X-ray crystal structure of mCherryTYG (PDB 6M3Z) with data collection and refinement statistics reported in Table S-2. The (A) overall structure of mCherryTYG crystallized at pH 8.5 is shown with (B) a close-up view of the chromophore environment. The $2|F_o|-|F_c|$ map contoured at 3 σ for the chromophore is shown as the blue cage. Electron density for the two major conformations of Glu215 is shown. (C) One conformation resembles that of Glu215 found in wildtype mCherry (PDB 2H5Q, grey overlay), and (D) the second conformation resembles mOrange (PDB 2H5O, grey overlay). Distances between atoms are labeled, and grey spheres are water molecules.

RESULTS AND DISCUSSION

Structural analysis of mCherryTYG. We solved the X-ray crystal structure of mCherryTYG to a resolution of 1.09 Å, which allowed us to unambiguously determine the maturation state of its chromophore (**Figure 1**). The mCherryTYG mutant contains the M66T mutation found in mOrange that causes an additional cyclization of its chromophore (**Figure S-1**) [50,53]. In mOrange the threonine mutation positions the side chain hydroxyl for a nucleophilic attack on the backbone amide, creating an oxazole ring. The oxaole ring partially disrupts the fully extended chromophore conjugation system found in DsRed-type RFPs, which results in the shift to orange color. Here, the M66T mutation has the same effect on chromophore maturation, generating an oxazole ring but in the context of the overall mCherry scaffold (**Figure 1**). This chromophore mutation did not significantly alter the overall structure of the protein as compared to the previously determined wildtype mCherry structure (0.098 Å root mean square deviation for the Cα atoms of residues 4-225) [50]. However, it still induces a shift in the pK_a of the chromophore (**Table S-1**), and protonation of the chromophore at near neutral pH causes a characteristic shift to a lower wavelength peak in the pH-dependent absorption spectrum (**Figure S-2**)[54]. Taken together, these results are consistent with the idea that the pK_a shift of the chromophore phenolic proton is caused primarily by decreased π-electron density in the conjugated chromophore system. In addition to the chromophore itself, structural differences were observed at residues Glu215, discussed below, and Lys70 (**Figure S-1**).

Comparison of our structure for mCherryTYG (pH 8.5) with those of wildtype mCherry (PDB 2H5Q, pH 8.5) and mOrange (PDB 2H5O, pH 8.2) reveal two distinct conformations for the glutamate 215 side chain, contributing to changes in the local electrostatic environment of the chromophore. In wildtype mCherry, the Glu215 side chain is within hydrogen bonding distance 2.7 Å from the imidazolinone ring nitrogen of the chromophore; however, in mOrange, this side chain is rotated 1 Å away from the chromophore nitrogen and instead hydrogen bonds with the interior network of waters. The electron density of mCherryTYG reveals ~50% occupancy of Glu215 in two conformations, one of which is consistent with wildtype mOrange and the other with mCherry (**Figure 1**). In the wildtype mCherry conformation Glu215 is protonated, acting as the hydrogen bond donor to the chromophore nitrogen; whereas in the mOrange conformation, Glu215 is deprotonated and acts as the acceptor in its hydrogen bond to water. Importantly, deprotonation of Glu215 is hypothesized to cause the hypsochromic shift in the absorbance and fluorescence spectra of wildtype mCherry at high pH[50]. The spectral shift observed for mCherryTYG is larger than the spectral shift observed for wildtype mCherry[27,50]. This larger shift is likely caused by the partial occupancy of Glu215 in the anionic state that results in a stronger local electric field

around the chromophore, shown to be a major factor in tuning the color of fluorescent proteins[55]. It is also evident that Glu215 in mCherryTYG is titratable in the physiological pH range (**Figure S-2**). Thus, in mCherryTYG the M66T chromophore mutation causes an increase in the structural dynamics of Glu215, which plays an important role in governing the pH-dependent electrostatic environment of the chromophore and is reflected in its steady-state spectral properties. As described below, this behavior did not negatively impact on our ability to use mCherryTYG as a pH sensor, as has been observed for other pH sensors like pHTomato[26].

Thus, our X-ray crystal structure of mCherryTYG provides a structural rationale for its steady-state fluorescence properties. Shu *et al*. also noted evidence of incomplete chromophore maturation with the M66T mutation in mOrange, evidenced by green fluorescence[50]. Importantly, we did not observe green fluorescence of mCherryTYG when it was purified for protein studies nor when expressed in bacteria or mammalian cells, showing that mCherryTYG matures efficiently (**Figure S-3**).

mCherryTYG is a fluorescence lifetime pH sensor. We next demonstrated that mCherryTYG is an effective pH sensor whether in purified protein or live cells. Steady-state spectroscopy of the protein in solution shows a pH dependence of both the extinction coefficient (ε) and fluorescence quantum yield (ϕ) of mCherryTYG (**Figure 2**). Due to acid quenching from pH 9.0 to pH 5.5, the extinction coefficient decreases from ε = 55,000 $M^{-1}cm^{-1}$ to ε = 20,000 $M^{-1}cm^{-1}$ and the fluorescence quantum yield decreases from ϕ = 0.31 to ϕ = 0.05, causing a greater than 16-fold change in brightness. Importantly, although dimming occurs in acidic conditions, even at pH 5.5 data acquisition was not encumbered, allowing for capture of a large biologically relevant pH range. With its large change in quantum yield, we hypothesized that mCherryTYG would exhibit a large change in fluorescence lifetime.

As hypothesized, time-resolved spectroscopy revealed that mCherryTYG shows an exceptionally large pH-dependent fluorescence lifetime change in protein solution studies. The mCherryTYG fluorescence decays were well fit with two exponential components, a fast decay component t_{fast} ~ 0.5 ns and a slow decay component t_{slow} ~ 3 ns (**Table S-3**). Importantly, the weighted average of the fitted components, which we simply refer to as the "lifetime", changes from 1.3 ns to 3.0 ns from pH 5.5 to pH 9.0, exhibiting a dynamic range with an unprecedented maximal 1.7 ns change and a pK_a of 6.8 (**Figure 2**). This dynamic range is 4-fold larger than the 0.4 ns lifetime change exhibited by the RFP pH sensor pHRed[28]. Notably, the apparent pK_a of 6.8 determined from lifetime measurements differs from the pK_a of 7.4 determined from steady-state brightness measurements (**Table 1**), which is expected because of the contribution of photon counting as described by Mongeon *et al*[56]. Interestingly, there is a reciprocal change in the amplitudes of the fast and slow components as the pH fluctuates. The slow decay component increases in its relative amplitude as pH increases, with an apparent pK_a of 6.8 in agreement with the pK_a determined from the lifetime response (**Figure S-4**). This trend correlates with acid quenching in which the equilibrium favors a protonated low quantum yield state. Given the promising results of our protein studies, we next determined if mCherryTYG would be effective for lifetime measurements when expressed in live cells.

To this end, we first established that the measurement of mCherryTYG's lifetime is not affected by total fluorescence intensity, determined by expression levels, or is it distorted by scatter, which is determined by culture density. It is known that strongly scattering media such as thick biological tissues

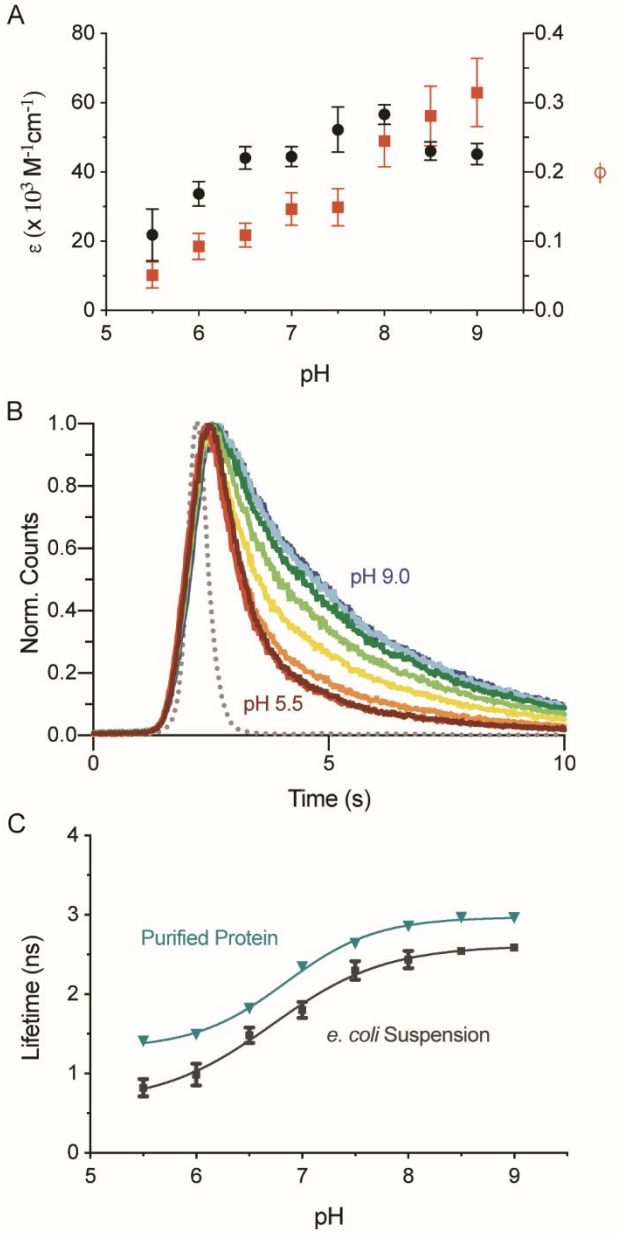

Figure 2. pH-dependent fluorescence lifetime of mCherryTYG. (A) The extinction coefficient (ε) and quantum yield (ϕ) are pH-dependent, but low pH does not completely quench fluorescence (mean ± std, n=3). (B) Representative fluorescence decays from time-resolved measurements of purified protein show that the fluorescence lifetime decreases with decreasing pH (grey dots, IRF). (C) The sensor exhibits a pK_a of 6.8 both in solution and expressed in live *E. coli* (mean ± std, n=3).

can affect the observed fluorescence lifetime[57,58]. However, typical bacterial suspensions should not cause a significant increase in the photon scattering path length relative to the magnitude of the fluorescence lifetime. Therefore, we expect the lifetime to be invariant over a range of liquid culture densities during the log growth phase. To demonstrate this, live cells expressing mCherryTYG were suspended in minimal M63 media at pH 7.5 at optical densities of 0.1 to 0.7, and total fluorescence intensity and fluorescence lifetime were measured under the same respective instrumental settings (**Figure 3**). The fluorescence of mCherryTYG was easily detectable at all densities. As expected, the lifetime did not significantly differ across a nearly 10-fold range of total fluorescence and scattering. Thus, the mCherryTYG lifetime offers a highly dependable approach to measuring physiological pH over a broad range of timescales and culture conditions.

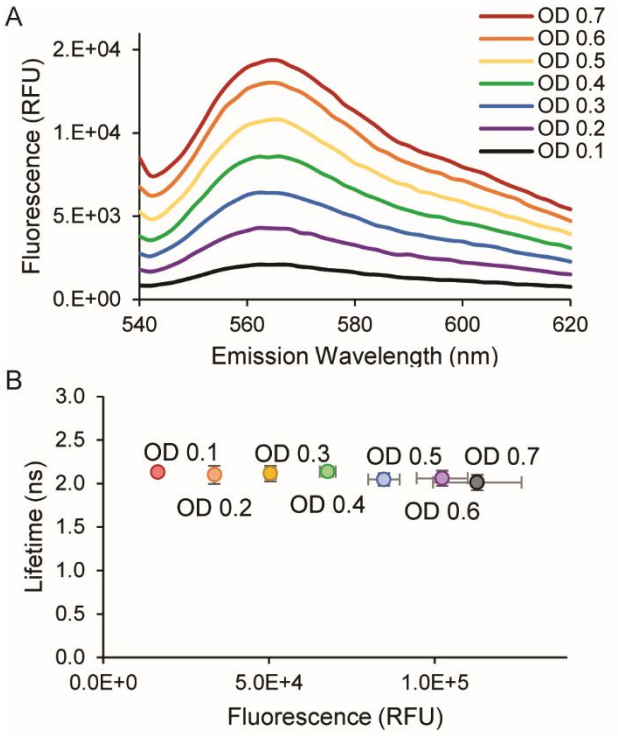

Figure 3. Fluorescence lifetime is independent of scatter and total intensity in live cell suspensions. (A) mCherryTYG fluorescence was detectable live-cell suspensions at an OD of 0.1 to 0.7. (B) The lifetime does not depend on the total fluorescence intensity or scatter (mean ± std, n = 3; no differences by ANOVA with Tukey's posthoc, p>0.4 for all comparisons).

Next, we validated that mCherryTYG exhibits its pH-dependent lifetime when expressed in live cells. It is well known that the local environment can alter fluorescent sensor properties due to interactions between proteins, membranes, or other cellular components[59,60]. However, fluorescent proteins offer a distinct advantage because the protein β-barrel surrounding the interior chromophore protects it from interactions with neighboring biomolecules. To test that pH sensing capability is preserved in live cells, we expressed mCherryTYG in the cytosol of *E. coli* and then measured the pH response in live cell suspensions. As previously established, we used benzoate and methylamine to equalize intracellular and extracellular pH in these experiments[41,42,61]. Significantly, we found that the mCherryTYG lifetime exhibits a pK_a of 6.8 regardless of its environment, whether as purified protein in dilute solution or expressed in the crowded intracellular environment of a live cell. Interestingly, in live cells there is an increase in dynamic range with a maximum 2 ns change compared to the 1.7 ns change of the purified protein. There is also a small decrease in the absolute lifetime values, with lifetimes ranging from 0.6 ns at pH 5.5 to 2.6 ns at pH 9.0 in live cells. It is possible that non-specific interactions between mCherryTYG and the cell could cause the shift in lifetime values, however mCherry is relatively inert[48]. Furthermore, mCherryTYG is quite pH selective, and it is not affected by differences in monovalent salts, divalent salts, or redox (**Figure S-2**). Alternatively, the overall decrease in lifetime is consistent with the higher index of refraction of cellular environments, which have been measured to cause lifetime shifts of up to ~0.5 ns compared to dilute protein solutions[62,63]. Notably, in live cells the mCherryTYG fluorescence is only partially quenched at pH 5.5, and fluorescence is still easily detectable for lifetime measurements. Thus, mCherryTYG is a well-behaved pH sensor that retains its pK_a in live cells with an exceedingly large fluorescence lifetime dynamic range.

Interestingly, we noticed that the media composition could greatly affect the basal lifetime of mCherryTYG when expressed in live cells. We suspected that mCherryTYG was reporting differences in metabolic activity, specifically respiration, that contribute to intracellular pH homeostasis of the aerobic cultures. Thus, the live-cell pH calibration curves were obtained under metabolic inhibition in the absence of exogenous energy sources and in the presence of cyanide to block respiration[64,65]. This resulted in highly reproducible pH response curves. Importantly, these observations suggested that we could use our sensor measurement approach to quantify pH fluctuations as a readout of metabolic activity in real-time, which we investigated next as a proof-of-concept application.

Live-Cell Lifetime Spectroscopy. Building on our sensor characterization, we set out to demonstrate that (1) mCherryTYG is effective for measuring physiology, (2) time-resolved spectroscopy on live-cell suspensions provides a quantitative approach to real-time continuous assays, and (3) mCherryTYG enables simultaneous multicolor lifetime measurements.

In regards to our first two objectives, we carried out single-color fluorescence lifetime measurements with mCherryTYG to quantify how respiration acutely contributes to pH regulation, which had not been directly determined in this manner previously. Under aerobic conditions, *E. coli* use a variety of pH homeostasis mechanisms to maintain intracellular pH in range of 7 - 8, even in the face of extreme acid or base stress[4,13–16]. Evolved acid stress resistance mechanisms include potassium-dependent proton extrusion, amino acid decarboxylation, as well as the upregulation of many genes including respiratory complex proteins[66,67]. Seminal work using radioactive tracer distribution demonstrated that respiration contributes to the substantial difference between intracellular and extracellular pH under

aerobic conditions[64], and live-cell nuclear magnetic resonance (NMR) studies showed that pH homeostasis effectively resists transient pH changes under acid and base challenge[68]. Under anaerobic conditions, live-cell NMR also established that ATP can be used to power proton efflux in the absence of respiration[65]. Here, we present a novel approach using mCherryTYG live-cell lifetime spectroscopy to demonstrate that respiration also contributes to acute pH regulation under aerobic conditions.

We first continuously measured the lifetime of mCherryTYG in live *E. coli* suspensions subjected to mild acid stress. Live cells were equilibrated in minimal M63 media buffered at pH 6 containing potassium but no amino acids and no exogenous energy sources[61]. As expected, at baseline in the absence

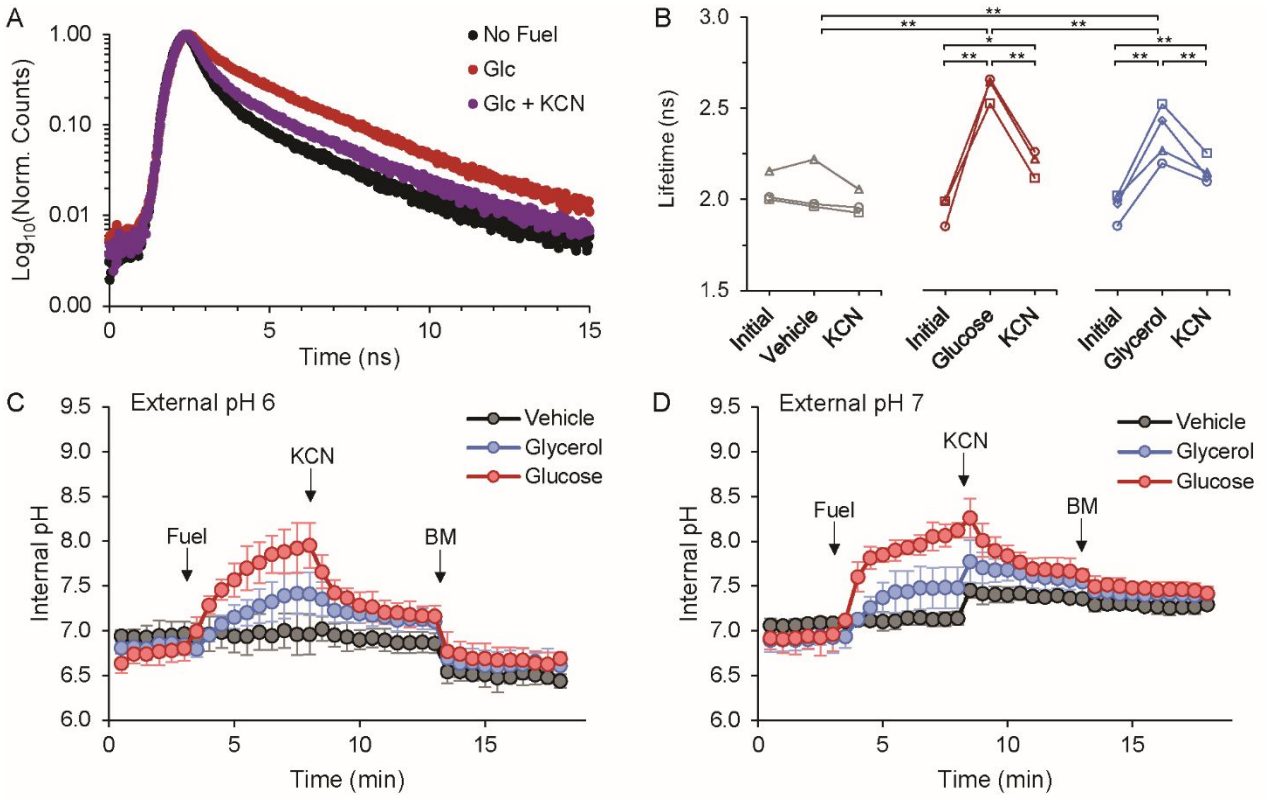

Figure 4. Fuel and respiration-dependent pH homeostasis. Time-resolved measurements of live *E. coli* expressing mCherryTYG in M63 media lacking glucose and amino acids, buffered at (A-C) pH 6 or (D) pH 7. (A) Example fluorescence lifetime decays. (B) Addition of Fuel, glucose (n=3) or glycerol (n=4), causes an increase in cytosolic pH reported by the mCherryTYG lifetime, but no-fuel Vehicle addition (n=3) does not. Cyanide (KCN) blocks respiration and causes acidification after loss of electron transport mediated proton pumping. Lines connect data for independent cultures. (**p<0.05, *p<0.1, two-tail t-test, paired within fuel condition, unpaired between fuels). (C-D) Time-dependent changes in intracellular pH for cells in M63 media at (C) pH 6 and (D) pH 7 (n=3 each). Data are the mean ± 95% confidence interval (CI) for independent cultures. Benzoate and methylamine (BM) equalize the intracellular and extracellular pH.

of fuel the cytosol was slightly acidic at pH = 6.5 - 7.0 (**Figure 4**, **S-5**). Upon addition of glucose, there was an immediate alkalinization of the cytosol with the intracellular pH approaching pH 8. The subsequent addition of cyanide to block respiration caused a pH reversal and acidification of the cytosol. Control cell suspensions expressing either no fluorescent protein or the pH-insensitive wildtype mCherry did not exhibit lifetime changes (**Figure S-5**). To demonstrate that mCherryTYG was well-calibrated, we added benzoate and methylamine at the end of the experiment to equialize the intracellular and extracellular pH [61]. Notably, mCherryTYG reported a pH of 6.5 which was consistent with the alkalinization of the M63 media caused by the addition of the potassium cyanide basic salt, as measured using pH electrodes for orthogonal validation. Of note, cyanide addition did not cause a pH change in the vehicle control without glucose addition (**Figure 4**, **S-5**), indicating minimal respiratory proton pumping activity in the absence of a fuel. However, in both the glucose and no fuel control conditions after cyanide treatment, the cytosol remained alkaline with respect to the

extracellular media, and benzoate and methylamine caused acidification after loss of the intracellular-extracellular pH gradient. Hence, the live cells also retained respiration-independent homeostatic mechanisms that persist in the absence of fuel. We observed a similar phenotype when *E. coli* were subjected to the same protocol using M63 media at pH 7 (**Figure 4**, **S-5**). Interestingly, with mild alkaline stress using M63 media at pH 8, the addition of glucose still caused a trend towards an alkalinization, though it was not statistically significant across independent cultures (**Figure S-5**). Thus, our measurements demonstrate that *E. coli* are able to resist mild acid stress and maintain a near neutral cytosol on acute timescales even in the absence of an external energy source. Furthermore, we hypothesize that the cyanide-inhibited alkalinization upon glucose addition reflects the fuel and respiration-dependent pumping of protons out of the cell to support oxidative phosphorylation and ATP synthesis.

To test that our experimental conditions do in fact result in intracellular ATP level changes, we utilized the ATeam1.03YEMK (abbreviated ATeam) fluorescent sensor which is well-tuned for bacterial ATP levels[69,70]. The sensor employs Förster-type resonance energy transfer (FRET) between a cyan fluorescent protein (CFP) and yellow fluorescent protein (YFP) donor-acceptor pair in which ATP-binding causes an increase in FRET[70]. The steady-state fluorescence emission spectra of live cell suspensions expressing ATeam were measured in the absence of fuel, after glucose addition, and after cyanide addition (**Figure 5**). The emission spectra showed significant increases in FRET from the resulting increase in intracellular ATP after glucose addition, which is reversed with the subsequent addition of cyanide. Thus, our time-resolved fluorescence measurements of mCherryTYG and steady-state fluorescence measurements of ATeam are consistent with fuel and respiration-dependent ATP synthesis.

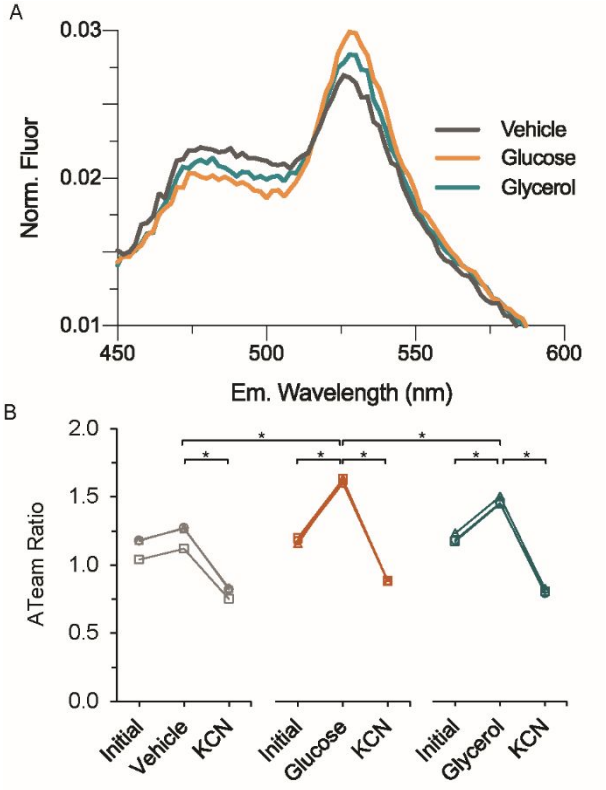

Figure 5. Acute changes in respiration regulates intracellular ATP. (A) Addition of glucose or glycerol increases intracellular ATP levels, reported by increased FRET-to-CFP peak ratios in the steady-state fluorescence emission spectra of live *E. coli* expressing ATeam1.03YEMK. (B) Glucose causes a greater increase in ATP compared to glycerol, and KCN decreases ATP. Lines connect data for independent cultures. (*p<0.01, 2-tailed t-test, n=3).

These results show that mCherryTYG is very effective a reporting pH changes linked to respiratory activity and central energy metabolism, and therefore we next tested whether we could quantify differences in fuel source. Previous studies have demonstrated that glycerol can support bacterial respiration, but it is a less efficient energy source that provides half the equivalents of ATP production compared to glucose[71–73]. We therefore hypothesized that using glycerol as fuel would result in a diminished respiration-dependent alkalinization compared to glucose. Employing the same experimental protocol, we measured the mCherryTYG lifetime in live cells and found that the addition of 0.8% glycerol[42] caused an alkalinization of the cytosol qualitatively similar to the response during glucose addition (**Figure 4**). However, the approximately equimolar addition of glycerol caused a stoichiometric attenuation in the pH increase compared to glucose addition (**Figure 4**). Furthermore, steady-state fluorescence emission spectra of cells expressing ATeam show that the increase in ATP is significantly lower for glycerol compared to glucose treatment (**Figure 5**). Cyanide treatment did cause a decrease in ATP levels, indicating that glycerol supports ATP production via respiratory activity. Notably, control experiments demonstrate that the pH sensitivity of the ATeam sensor[70] does not account for the observed ratio changes, and ATeam faithfully reports ATP

levels under these conditions (**Figure S-6**). Thus, the use of glycerol compared to glucose as an energy source results in a quantitative decrease in ATP production that correlates well with a decrease in respiration-dependent proton efflux.

Using our sensor approach, we have now measured to what extent respiration can contribute to the regulation of intracellular pH on acute time scales under aerobic conditions. Overall, these results demonstrate that continuous real-time measurements of mCherryTYG lifetime in live-cell suspensions can provide new and quantitative insights into the metabolic regulation of pH. In these experiments, we validated the effects on energy metabolism using steady-state fluorescence measurements of the ATeam sensor. However, mCherryTYG is a significant addition to the toolbox of genetically-encoded pH sensors, not only because it provides a lifetime-based readout, but because it is red fluorescent, making it spectrally compatible with other sensors. We demonstrate this advantage next with simultaneous multicolor spectroscopy.

Multicolor Live-Cell Lifetime Spectroscopy. To address the third objective of our proof-of-concept studies, we showed that mCherryTYG is spectrally compatible for simultaneous two-color lifetime measurements, facilitating direct correlative analysis of more than one physiological parameter within the same specimen. Our steady-state spectroscopy results demonstrated that the ATeam detects changes in ATP levels related to the pH fluctuations reported by mCherryTYG. Because ATeam is a FRET-based sensor, the CFP donor lifetime should also change with respect to ATP levels. The ATP-bound, high FRET state should have a decreased CFP donor lifetime, and therefore an increase in ATP will cause a decrease in the ATeam lifetime. Therefore, it should be possible to measure the lifetimes of ATeam and mCherryTYG simultaneously. To test this, we studied *E. coli* cultures with a mixture of cells expressing mCherryTYG and cells expressing ATeam.

As expected, in M63 media at pH 6, the addition of glucose causes an increase in the mCherryTYG lifetime because of cytosolic alkalinization (**Figure 6**, **S-7**). Importantly, glucose addition also causes a concurrent decrease in the ATeam lifetime, reporting an increase in ATP within the same sample (**Figure 6**, **S-7**). The subsequent addition of cyanide blocks respiration causing re-acidification of the cytosol, and there is a correlated increase in the ATeam lifetime that reports a decrease in intracellular ATP levels with metabolic inhibition. Hence, lifetime changes of both mCherryTYG and ATeam can be measured simultaneously to directly correlate changes in respiratory proton pumping and ATP synthesis.

We were then curious how different nutrient additives found in bacterial medias might affect metabolism. For example, casamino acids are typically used to provide amino acid supplementation and support nitrogen metabolism in microbial cultures. Interestingly, we found the addition of 0.2% casamino acids[18] in either the absence or presence of glucose caused a similar increase in the mCherryTYG lifetime that is reversed by cyanide treatment (**Figure 6**, **S-7**), showing that casamino acids can support respiratory proton pumping. However, the ATeam lifetime also increased, indicating an acute consumption of ATP that was further exacerbated by cyanide addition (**Figure 6**, **S-7**). We hypothesized It is possible that the consumption of ATP results from saturation of amino acid influx pathways via energy-dependent ABC transporters as well as flux through previously depleted anapleurotic and biosynthetic pathways. However, casamino acids are not a chemically-defined mixture, and in the future beyond this proof-of-concept, it will be interesting to tease apart the microbial metabolism responsible for these observations.

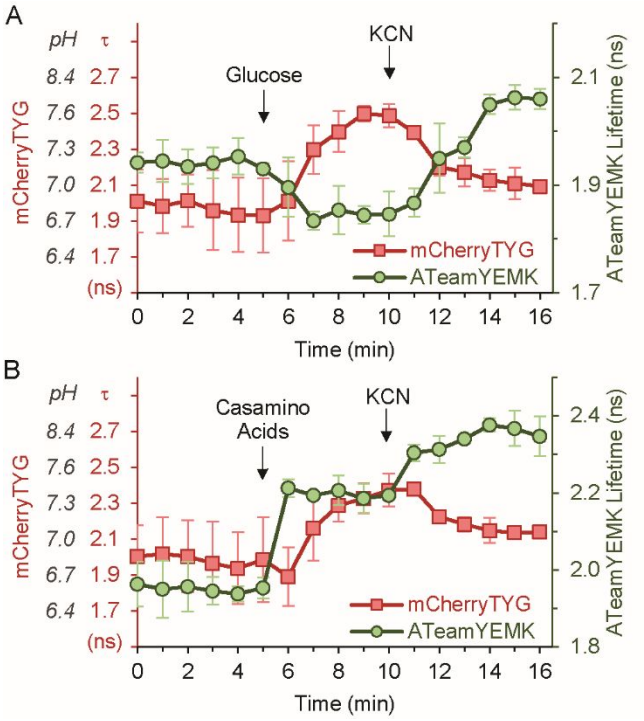

Figure 6. Simultaneous two-color live-cell lifetime measurements directly correlate intracellular pH and ATP levels. Live *E. coli* expressing mCherryTYG (red) and ATeam (green) were mixed in M63 media at pH 6. (A) Glucose addition causes an increase in pH and the mCherryTYG lifetime (τ). It also causes an increase in ATP and thus a decrease in ATeam CFP donor lifetime (green). Block of respiration with cyanide causes a reversal. (B) Casamino acids support respiratory alkalinization reported by the increase in the mCherryTYG lifetime, but the increase in ATeam lifetime indicates acute ATP consumption (mean ± 95% CI, n=3).

Ultimately, respiration supports the generation of a pH gradient that contributes to the proton motive force driving ATP synthesis. Therefore we used mCherryTYG and EGFP to measure different changes in intracellular and extracellular pH simultaneously. EGFP is pH sensitive, and acidification causes a decrease in its lifetime[37,74,75]. Cells expressing mCherryTYG were equilibrated in M63 media modified to contain 5 mM MOPS, providing weak buffering capacity at pH 8. Purified EGFP was included in the media, with no amino acids or fuel present. Measuring mCherryTYG and EGFP lifetimes simultaneously, we first added 50 mM MES to acidify the extracellular media to pH 6 (**Figure 7**, **S-8**). Both green and red fluorescence lifetimes decreased, reflecting the acidification of both the media and cytosol, respectively. Interestingly, the mCherryTYG lifetime reported a reproducible acid transient indicative of fast regulation that, taken together with our previous observations, supports the

persistence of fuel and respiration-independent homeostatic mechanisms. Such mechanisms could rely on decarboxylase acid resistance systems, given the short starvation likely did not completely deplete residual glutamate and arginine. Upon the addition of glucose, however, the extracellular pH remained constant as reported by EGFP, while the intracellular pH increased as reported by mCherryTYG. Furthermore, the addition of the cyanide basic salt caused an alkalinization of the extracellular pH as expected, and also expected was the blockade of respiration causing an acidification of the cytosol. These results clearly demonstrate that mCherryTYG and EGFP lifetimes can be measured in live-cell suspensions to simultaneously quantify intracellular and extracellular pH, providing quantitative insight into respiratory contribution to the generation of the proton gradient.

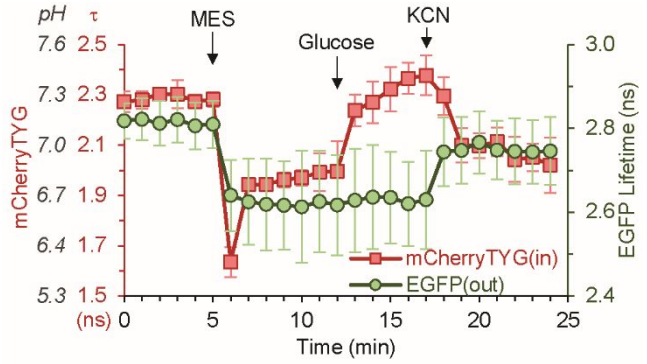

Figure 7. Simultaneous measurement of the extracellular and intracellular pH. Live *E. coli* expressing mCherryTYG (red) were suspended in M63 media at pH 8 containing purified EGFP (green). The media was first acidified to pH 6 with MES, followed by the addition of glucose and KCN (mean ± 95%CI, n=3).

CONCLUSIONS

Understanding pH regulation is fundamentally important to deconvoluting the complex physiology of species ranging from single-cell prokaryotes to mammals. In this report, we were able to study metabolically-driven pH changes in live *E. coli* using mCherryTYG, which we demonstrate is a highly effective genetically-encoded red fluorescent sensor, that quantitatively reports pH via its fluorescence lifetime. Using this sensor, we make novel measurements of the acute contributions of respiration to intracellular pH homeostasis in support of ATP generation. Our results clearly demonstrate that lifetime spectroscopy of mCherryTYG could be used to quantify the contributions of different homeostatic mechanisms under different nutrient and growth conditions. Furthermore, the mCherryTYG pH sensor stands out uniquely as a red fluorescent lifetime pH sensor. In comparison to the only other RFP lifetime pH sensor characterized in live cells, the 2.0 ns dynamic range of mCherryTYG is a vast improvement over the 0.4 ns dynamic range of pHRed[28]. In fact, the 2.0 ns dynamic range of mCherryTYG is extraordinarily large for any lifetime sensor, including: EGFP that exhibits a 0.8 ns pH-dependent change[37,74,75]; intramolecular FRET sensors such as the AKAR protein kinase A[76,77], IDOCKS protein kinase C[78], and epac cAMP[79] sensors that exhibit 0.2 ns, 0.3 ns, and 1.0 ns changes, respectively; and intermolecular FRET small GTPase activity sensors that exhibit 0.3 ns changes[80]. Additionally, we found that neither the pK_a or dynamic range of mCherryTYG was strongly perturbed by expression in live cells, unlike many other sensors that experience significant changes in analyte sensitivity as well as attenuated dynamic ranges[81,82]. Thus, in general our methodology fills an important technology gap that provides molecular specificity in the live-cell context without the high barriers of FLIM instrumentation.

ASSOCIATED CONTENT

Supporting Information

The Supporting Information is available free of charge on the ACS Publications website.

Figures S-1 through S-7, Table S-1, and Table S-2 as described in the text (PDF)

AUTHOR INFORMATION

Corresponding Author

* E-mail: mtantama@purdue.edu

ORCID

Emily Haynes: 0000-0003-4312-2852
Megha Rajendran: 0000-0001-8078-4738
Angeline Lyon: 0000-0001-7501-0148
Mathew Tantama: 0000-0002-4072-7680

Present Addresses

†Section on Molecular Transport, Eunice Kennedy Shriver National Institute of Child Health and Human Development, National Institutes of Health, Bethesda, MD, 20892, USA.

Author Contributions

All authors contributed to the execution of experiments. E.H. and A.M.L. carried out crystallization studies and solved the crystal structure. E.H. and M.T. wrote the manuscript with input from all authors. ‡These authors contributed equally.

Notes

The authors declare no competing financial interest.

ACKNOWLEDGMENT

This work was supported by National Institutes of Health Grants R21 NS092010 and R21 EY026425 to M.T. and 1R01HL141076-01 to A.M.L.; American Heart Association Scientist Development Grant 16SDG29930017 to A.M.L., and an American Cancer Society Institutional Research Grant (IRG-14-190-56) to the Purdue University Center for Cancer Research (A.M.L). The content is solely the responsibility of the authors and does not necessarily reflect the official views of the National Heart, Lung, and Blood Institute, or the National Institutes of Health. Use of the Advanced Photon Source, an Office of Science User Facility operated for the U. S. Department of Energy (DOE) Office of Science by Argonne National Laboratory, was supported by the U.S. DOE under Contract Number DE-AC02-06CH11357. We thank the LS-CAT staff members for their help with data collection. We thank Nicholas Noinaj for assistance with model refinement and the PDB structure deposit. Coordinates and structure factors for mCherryTYG are deposited in the Protein Data Bank as 6M3Z.

REFERENCES

(1) Berezin, M. Y.; Achilefu, S. *Chem. Rev.* **2010**, *110*, 2641–2684.

(2) Hum, J.; Siegel, A.; Pavalko, F.; Day, R. *Int. J. Mol. Sci.* **2012**, *13*, 14385–14400.

(3) Goh, G. B.; Laricheva, E. N.; Brooks, C. L. *J. Am. Chem. Soc.* **2014**, *136*, 8496–8499.

(4) Krulwich, T. A.; Sachs, G.; Padan, E. *Nat. Rev. Microbiol.* **2011**, *9*, 330–343.

(5) Farha, M. A.; French, S.; Stokes, J. M.; Brown, E. D. *ACS Infect. Dis.* **2018**, *4*, 382–390.

(6) Zhao, N.; Darby, C. M.; Small, J.; Bachovchin, D. A.; Jiang, X.; Burns-Huang, K. E.; Botella, H.; Ehrt, S.; Boger, D. L.; Anderson, E. D.; et al. *ACS Chem. Biol.* **2015**, *10*, 364–371.

(7) Chan, L. C. Z.; Khalili Moghaddam, G.; Wang, Z.; Lowe, C. R. *ACS Sensors* **2019**, *4*, 456–463.

(8) Luo, X.; Yang, H.; Wang, H.; Ye, Z.; Zhou, Z.; Gu, L.; Chen, J.; Xiao, Y.; Liang, X.; Qian, X.; et al. *Anal. Chem.* **2018**, *90*, 5803–5809.

(9) Paredes, J. M.; Idilli, A. I.; Mariotti, L.; Losi, G.; Arslanbaeva, L. R.; Sato, S. S.; Artoni, P.; Szczurkowska, J.; Cancedda, L.; Ratto, G. M.; et al. *ACS Chem. Biol.* **2016**, *11*, 1652–1660.

(10) Kinchen, J. M.; Ravichandran, K. S. *Nat. Rev. Mol. Cell Biol.* **2008**, *9*, 781–795.

(11) Gao, W.; Chan, J. M.; Farokhzad, O. C. *Mol. Pharm.* **2010**, *7*, 1913–1920.

(12) Su, H.; Xu, G.; Chen, H.; Xu, Y. *ACS Sustain. Chem. Eng.* **2015**, *3*, 2002–2011.

(13) Padan, E.; Bibi, E.; Ito, M.; Krulwich, T. A. *Biochim. Biophys. Acta - Biomembr.* **2005**, *1717*, 67–88.

(14) Lund, P.; Tramonti, A.; De Biase, D. *FEMS Microbiol. Rev.* **2014**, *38*, 1091–1125.

(15) Foster, J. W. *Nat. Rev. Microbiol.* **2004**, *2*, 898–907.

(16) Slonczewski, J. L.; Fujisawa, M.; Dopson, M.; Krulwich, T. A. *Adv. Microbial Physiol.* **2009**, 55, 1–317.

(17) Meylan, S.; Porter, C. B. M.; Yang, J. H.; Belenky, P.; Gutierrez, A.; Lobritz, M. A.; Park, J.; Kim, S. H.; Moskowitz, S. M.; Collins, J. J. *Cell Chem. Biol.* **2017**, *24*, 195–206.

(18) Lobritz, M. A.; Belenky, P.; Porter, C. B. M.; Gutierrez, A.; Yang, J. H.; Schwarz, E. G.; Dwyer, D. J.; Khalil, A. S.; Collins, J. J. *Proc. Natl. Acad. Sci.* **2015**, *112*, 8173–8180.

(19) Wencel, D.; Abel, T.; McDonagh, C. *Anal. Chem.* **2014**, *86*, 15–29.

(20) Han, J.; Burgess, K. *Chem. Rev.* **2010**, *110*, 2709–2728.

(21) Greenwald, E. C.; Mehta, S.; Zhang, J. *Chem. Rev.* **2018**, *118*, 11707–11794.

(22) Szmacinski, H.; Lakowicz, J. R. *Anal. Chem.* **1993**, *65*, 1668–1674.

(23) Miesenböck, G.; De Angelis, D. A.; Rothman, J. E. *Nature* **1998**, *394*, 192–195.

(24) Poburko, D.; Santo-Domingo, J.; Demaurex, N. *J. Biol. Chem.* **2011**, *286*, 11672–11684.

(25) Johnson, D. E.; Ai, H.-W.; Wong, P.; Young, J. D.; Campbell, R. E.; Casey, J. R. *J. Biol. Chem.* **2009**, *284*, 20499–20511.

(26) Li, Y.; Tsien, R. W. *Nat. Neurosci.* **2012**, *15*, 1047–1053.

(27) Shen, Y.; Rosendale, M.; Campbell, R. E.; Perrais, D. *J. Cell Biol.* **2014**, *207*, 419–432.

(28) Tantama, M.; Hung, Y. P.; Yellen, G. *J. Am. Chem. Soc.* **2011**, *133*, 10034–10037.

(29) Gandasi, N. R.; Vestö, K.; Helou, M.; Yin, P.; Saras, J.; Barg, S. *PLoS One* **2015**, *10*, e0127801.

(30) Sankaranarayanan, S.; De Angelis, D.; Rothman, J. E.; Ryan, T. A. *Biophys. J.* **2000**, *79*, 2199–2208.

(31) Boens, N.; Qin, W.; Basarić, N.; Hofkens, J.; Ameloot, M.; Pouget, J.; Lefèvre, J.-P.; Valeur, B.; Gratton, E.; VandeVen, M.; et al. *Anal. Chem.* **2007**, *79*, 2137–2149.

(32) Lakowicz, J. R.; Szmacinski, H.; Nowaczyk, K.; Johnson, M. L. *Proc. Natl. Acad. Sci. U. S. A.* **1992**, *89*, 1271–1275.

(33) Wang, X. F.; Uchida, T.; Minami, S. A *Appl. Spectrosc.* **1989**, *43*, 840–845.

(34) Li, L.; Zhang, C.; Wang, P.; Wang, A.; Zhou, J.; Chen, G.; Xu, J.; Yang, Y.; Zhao, Y.; Zhang, S.; et al. *Anal. Chem.* **2019**, acs.analchem.8b04292.

(35) Ge, L.; Tian, Y. *Anal. Chem.* **2019**, acs.analchem.8b03992.

(36) Kneen, M.; Farinas, J.; Li, Y.; Verkman, A. S. Green *Biophys. J.* **1998**, *74*, 1591–1599.

(37) Nakabayashi, T.; Wang, H.-P.; Kinjo, M.; Ohta, N. *Photochem. Photobiol. Sci.* **2008**, *7*, 668.

(38) Esposito, A.; Gralle, M.; Dani, M. A. C.; Lange, D.; Wouters, F. S. *Biochemistry* **2008**, *47*, 13115–13126.

(39) Dean, K. M.; Davis, L. M.; Lubbeck, J. L.; Manna, P.; Friis, P.; Palmer, A. E.; Jimenez, R. *Anal. Chem.* **2015**, *87* , 5026–5030.

(40) Houston, J. P.; Yang, Z.; Sambrano, J.; Li, W.; Nichani, K.; Vacca, G. *Methods Mol. Biol.* **2018**, 1678, 421–446.

(41) Kitko, R. D.; Wilks, J. C.; Garduque, G. M.; Slonczewski, J. L. *PLoS One* **2010**, *5*, e10078.

(42) Wilks, J. C.; Slonczewski, J. L. *J. Bacteriol.* **2007**, *189*, 5601–5607.

(43) Kitko, R. D.; Cleeton, R. L.; Armentrout, E. I.; Lee, G. E.; Noguchi, K.; Berkmen, M. B.; Jones, B. D.; Slonczewski, J. L. *PLoS One* **2009**, *4* , e8255.

(44) Isom, D. G.; Page, S. C.; Collins, L. B.; Kapolka, N. J.; Taghon, G. J.; Dohlman, H. G. *J. Biol. Chem.* **2018**, *293* , 2318–2329.

(45) Aresta-Branco, F.; Cordeiro, A. M.; Marinho, H. S.; Cyrne, L.; Antunes, F.; de Almeida, R. F. M. *J. Biol. Chem.* **2011**, *286*, 5043–5054.

(46) Kirkpatrick, N. D.; Zou, C.; Brewer, M. A.; Brands, W. R.; Drezek, R. A.; Utzinger, U. *Photochem. Photobiol.* **2004**, *81*, 125–134.

(47) Ravichandra, B.; Joshi, P. G. *Biophys. Chem.* **1999**, *76*, 117–132.

(48) Cranfill, P. J.; Sell, B. R.; Baird, M. A.; Allen, J. R.; Lavagnino, Z.; de Gruiter, H. M.; Kremers, G.-J.; Davidson, M. W.; Ustione, A.; Piston, D. W. *Nat. Methods* **2016**, *13*, 557–562.

(49) Storoni, L. C.; McCoy, A. J.; Read, R. J. *Acta Crystallogr. Sect. D Biol. Crystallogr.* **2004**, *60*, 432–438.

(50) Shu, X.; Shaner, N. C.; Yarbrough, C. A.; Tsien, R. Y.; Remington, S. J. *Biochemistry* **2006**, *45*, 9639–9647.

(51) Emsley, P.; Lohkamp, B.; Scott, W. G.; Cowtan, K. *Acta Crystallogr. Sect. D Biol. Crystallogr.* **2010**, *66*, 486–501.

(52) Adams, P. D.; Afonine, P. V.; Bunkóczi, G.; Chen, V. B.; Davis, I. W.; Echols, N.; Headd, J. J.; Hung, L. W.; Kapral, G. J.; Grosse-Kunstleve, R. W.; et al. *Acta Crystallogr. Sect. D Biol. Crystallogr.* **2010**, *66*, 213–221.

(53) Shaner, N. C.; Campbell, R. E.; Steinbach, P. A.; Giepmans, B. N. G.; Palmer, A. E.; Tsien, R. Y. *Nat. Biotechnol.* **2004**, *22*, 1567–1572.

(54) Rajendran, M.; Claywell, B.; Haynes, E. P.; Scales, U.; Henning, C. K.; Tantama, M. *ACS Omega* **2018**, *3*, 9476–9486.

(55) Drobizhev, M.; Tillo, S.; Makarov, N. S.; Hughes, T. E.; Rebane, A. *J. Phys. Chem. B* **2009**, *113*, 12860–12864.

(56) Mongeon, R.; Venkatachalam, V.; Yellen, G. *Antioxid. Redox Signal.* **2016**, *25*, 553–563.

(57) Hutchinson, C. L.; Lakowicz, J. R.; Sevick-Muraca, E. M. *Biophys. J.* **1995**, *68*, 1574–1582.

(58) Kuwana, E.; Sevick-Muraca, E. M. *Anal. Chem.* **2003**, *75*, 4325–4329.

(59) Draxler, S.; Lippitsch, M. E. *Anal. Chem.* **1996**, *68*, 753–757.

(60) Nakabayashi, T.; Wang, H.-P.; Tsujimoto, K.; Miyauchi, S.; Kamo, N.; Ohta, N. *Chem. Lett.* **2007**, *36*, 206–207.

(61) Martinez, K. A.; Kitko, R. D.; Mershon, J. P.; Adcox, H. E.; Malek, K. A.; Berkmen, M. B.; Slonczewski, J. L. *Appl. Environ. Microbiol.* **2012**, *78*, 3706–3714.

(62) Balaev, A. E.; Dvoretski, K. N.; Doubrovski, V. A. *Proc. SPIE* **2002**, 4707, 253–260.

(63) Tregidgo, C.; Levitt, J. A.; Suhling, K. *J. Biomed. Opt.* **2008**, *13*, 031218.

(64) Padan, E.; Zilberstein, D.; Rottenberg, H. *Eur. J. Biochem.* **1976**, *63*, 533–541.
(65) Navon, G.; Ogawa, S.; Shulman, R. G.; Yamane, T. *Proc. Natl. Acad. Sci. U. S. A.* **1977**, *74*, 888–891.
(66) Maurer, L. M.; Yohannes, E.; Bondurant, S. S.; Radmacher, M.; Slonczewski, J. L. *J. Bacteriol.* **2005**, *187*, 304–319.
(67) Kannan, G.; Wilks, J. C.; Fitzgerald, D. M.; Jones, B. D.; BonDurant, S. S.; Slonczewski, J. L. *BMC Microbiol.* **2008**, *8*, 37.
(68) Slonczewski, J. L.; Rosen, B. P.; Alger, J. R.; Macnab, R. M. *Proc. Natl. Acad. Sci. U. S. A.* **1981**, *78*, 6271–6275.
(69) Yaginuma, H.; Kawai, S.; Tabata, K. V.; Tomiyama, K.; Kakizuka, A.; Komatsuzaki, T.; Noji, H.; Imamura, H. *Sci. Rep.* **2015**, *4*, 6522.
(70) Imamura, H.; Nhat, K. P. H.; Togawa, H.; Saito, K.; Iino, R.; Kato-Yamada, Y.; Nagai, T.; Noji, H. *Proc. Natl. Acad. Sci. U. S. A.* **2009**, *106*, 15651–15656.
(71) Kaleta, C.; Schäuble, S.; Rinas, U.; Schuster, S. *Biotechnol. J.* **2013**, *8*, 1105–1114.
(72) Bennett, B. D.; Kimball, E. H.; Gao, M.; Osterhout, R.; Van Dien, S. J.; Rabinowitz, J. D. *Nat. Chem. Biol.* **2009**, *5*, 593–599.
(73) Yao, R.; Xiong, D.; Hu, H.; Wakayama, M.; Yu, W.; Zhang, X.; Shimizu, K. *Biotechnol. Biofuels* **2016**, *9*, 175.
(74) Heikal, A. A.; Hess, S. T.; Webb, W. W. *Chem. Phys.* **2001**, *274*, 37–55.
(75) Li, W.; Houston, K. D.; Houston, J. P. *Sci. Rep.* **2017**, *7*, 40341.
(76) Tang, S.; Yasuda, R. *Neuron* **2017**, *93*, 1315–1324.
(77) Chen, Y.; Saulnier, J. L.; Yellen, G.; Sabatini, B. L. *Front. Pharmacol.* **2014**, *5*, 56.
(78) Colgan, L. A.; Hu, M.; Misler, J. A.; Parra-Bueno, P.; Moran, C. M.; Leitges, M.; Yasuda, R. *Nat. Neurosci.* **2018**, *21*, 1027–1037.
(79) Van der Krogt, G. N. M.; Ogink, J.; Ponsioen, B.; Jalink, K. *PLoS One* **2008**, *3*.
(80) Laviv, T.; Kim, B. B.; Chu, J.; Lam, A. J.; Lin, M. Z.; Yasuda, R. *Nat. Methods* **2016**, *13*, 989–992.
(81) Takanaga, H.; Chaudhuri, B.; Frommer, W. B. *Biochim. Biophys. Acta - Biomembr.* **2008**, *1778*, 1091–1099.
(81) Marvin, J. S.; Borghuis, B. G.; Tian, L.; Cichon, J.; Harnett, M. T.; Akerboom, J.; Gordus, A.; Renninger, S. L.; Chen, T.-W.; Bargmann, C. I.; et al. *Nat. Methods* **2013**, *10*, 162–170.

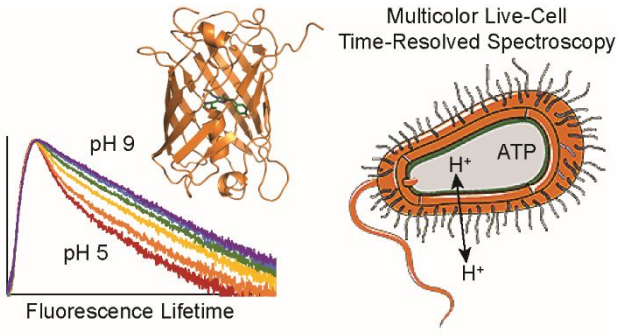

For Table of Contents Only